



# Synergistic adsorption of methylene blue using ternary composite of phosphoric acid geopolymer, calcium alginate, and sodium lauryl sulfate

Muhammad Irfan Khan<sup>1,2</sup> · Suriati Sufian<sup>1,2</sup> · Rashid Shamsuddin<sup>4</sup> · Muhammad Farooq<sup>3</sup> · Nabilah Saafie<sup>1,2</sup>

Received: 29 December 2023 / Accepted: 30 April 2024

© The Author(s), under exclusive licence to Springer-Verlag GmbH Germany, part of Springer Nature 2024

## Abstract

The removal of dyes from the aquatic ecosystem is necessary being a major threat to life. For enhanced remediation of methylene blue (MB) dye, a new ternary biopolymer-geopolymer-surfactant composite adsorbent is synthesized by combining phosphoric acid geopolymer (PAGP), calcium alginate (Alg), and sodium lauryl sulfate (SLS). During the synthesis of the composites, PAGP and SLS were mixed with the alginate matrix, producing porous hybrid beads. The PAGP-SLS-alginate (PSA) beads prepared were characterized using different analytical tools, i.e., scanning electron microscopy (SEM), Fourier transform infrared spectrophotometry (FTIR), X-ray diffractometry (XRD), surface area and porosimetry (SAP), and thermogravimetric analysis (TGA). To ascertain the ideal conditions for the adsorption process, a batch reactor procedure was used to investigate the effects of several parameters on MB adsorption, including pH (2, 4, 6, 8, 10), PSA adsorbent dosage (0.06–0.12 g), MB concentration (50–500 mg/L), contact time (15 to 300 min), and temperature (25, 35, and 45 °C). The SEM investigation indicated that ~1860 μm-sized PSA beads with 6–8 μm voids are generated. Based on XRD, FTIR, and SAP examinations, the material is amorphous, having numerous functional groups and an average pore size of 6.42 nm. Variation of pH has a little effect on the adsorption process, and the pH of 7.44 was found to be the  $pH_{pzc}$  of the PSA beads. According to the findings of the batch study, equilibrium adsorption was obtained in 270–300 min, showing that the adsorption process was moderately slow-moving and effective. The dye adsorption linearly increased with initial dye concentration over concentration range of 50–500 mg/L and reciprocally decreased with rise in temperature. 0.06 g adsorbent dose, 25 °C, pH10, and 270 min were found to be the better conditions for adsorption experiments. Langmuir isotherm fitted well compared to Freundlich, Temkin, and Dubinin-Radushkevich (DR) isotherm models on the experimental data, and the maximum adsorption capacity ( $q_{max}$ ) calculated was 1666.6 mg. g<sup>-1</sup>. Pseudo-second-order (PSO) kinetics model and multi steps (two) intra particle diffusion (IPD) model fitted well on the adsorption kinetics data. The system's entropy, Gibbs free energy, and change in enthalpy were measured and found to be -109.171 J. mol<sup>-1</sup>. K<sup>-1</sup>, -8.198 to -6.014 kJ. mol<sup>-1</sup>, and -40.747 kJ. mol<sup>-1</sup>. Thermodynamics study revealed that adsorption process is exothermic, energetically favorable and resulting in the decrease in randomness. Chemisorption is found to be the dominant mechanism as confirmed by pH effect, Langmuir isotherm, PSO kinetics, IPD model, and thermodynamics parameters. PSA beads were successfully regenerated using ethanol in a course of 120 min and re-used for five times. To sum up, the PSA adsorbent's impressive adsorption capability of 1666.66 mg/g highlights its potential as a successful solution for methylene blue removal. The results of this study add to the expanding corpus of information on sophisticated adsorption materials and demonstrate PSA's potential for real-world uses in wastewater treatment and environmental clean-up.

**Keywords** Adsorption · Alginate · Kinetics · Methylene blue · Phosphoric acid-based geopolymer · Thermodynamics

---

Responsible Editor: Tito Roberto Cadaval Jr

Extended author information available on the last page of the article

Published online: 02 July 2024

Springer

## Introduction

The rapid advancements observed in industrialization across the developing nations resulted in significant volumes of industrial wastewater being released into natural water sources without adequate treatment. This poses a severe risk to the well-being of aquatic organisms, flora, fauna, and public safety (Mahmoudian et al. 2023; Oladoye et al. 2022; Siyal et al. 2018). The demand for synthetic dyes, especially in the textile and apparel sectors, has led to a notable rise in their production. These chemical dyes are manufactured on a large scale each year, amounting to thousands of tons worldwide (Katheresan et al. 2018). Several techniques have been utilized for the wastewater treatment, encompassing electrochemical processes, bio-electro-degradation, electro-coagulation, ion-exchange, filtration, membranous separation, sedimentation, flocculation, adsorption, and photodegradation among others (Benkhaya et al. 2022; Candamano et al. 2023; Katheresan et al. 2018; Yousefi et al. 2024, 2021, 2019). Adsorption is the method of choice for dyes removal from waste water as approximately 58% of the studies has used adsorption (Dutta et al. 2021). Twenty-five percent of the studies has utilized various types of polymeric adsorbents whereas contribution of activated carbon is 23.9% (Dutta et al. 2021). Among other materials are hybrid materials, nano composites, biosorbents, metal oxide, and graphitic materials.

Hybrid materials (inorganic/organic) have recently undergone an amazing development in the realm of materials science. Hybrid materials contain a minimum of one organic phase and one inorganic phase, which combine to form hybrid substance having special features (Sharp 1998). In general, the inorganic part contributes to the thermal stability and mechanical strength, whereas the organic component imparts specialized properties (physical and/or chemical), including chemical reactivity, electrical, optical, and coherence (Pingan et al. 2017). Hybrid materials are emerging as practical options for the development of versatile systems with a broad range of functions due to the synergistic effects of their elements. Biomaterials, electrolytes, semiconductors, adsorbents, catalysts, biosensors, and drug delivery agents represent the diverse applications of these multifunctional systems. Hybrid polymers, recognized for their versatility, emerge as promising materials with diverse applications (Ge et al. 2017). The flexibility of hybrid polymer composites to be tailored to fulfil needs is one of its main benefits. The material can be specially crafted by designers to satisfy performance needs by combining various polymers, fibers, and nanoparticles. These materials are lightweight and offer superior corrosion and chemical resistance, making

them suitable in challenging conditions. Recently, various types of hybrid polymeric composites have been reported. One of recently introduced class, geopolymer-polymer hybrid materials has revealed promising properties in terms of mechanical strength, water resistivity, adsorption ability, and recyclability (Provis 2014; Provis and Bernal 2014). Geopolymers are of two types, i.e., acid- and alkali-activated geopolymers. Alkali-activated geopolymer is one of the most studied class that is formed as a result of the reaction of sodium hydroxide and silica glass with fly ash, metakaolin, or any other suitable materials (Lemoungna et al. 2016).

Phosphoric acid-based geopolymer (PAGP) uses phosphoric acid as the activator rather than alkaline solutions as used in most of the geopolymer formulations (Khan et al. 2015). Geopolymers based on phosphoric acid have demonstrated exceptional thermal stability and strong acid resistance, making them appropriate materials for industrial applications, such as cements, composites, fire-resistant coatings, and adsorbents for treating waste water (Shehata et al. 2021). Like alkali-activated geopolymers, alumina and silica-rich materials, e.g., fly ash and metakaolin are utilized as starting materials for the formulation of PAGPS (Celerier et al. 2018). Geopolymers have been used in various forms for wastewater treatment, e.g., adsorbents, membranes, and photocatalysts, but their lower adsorption capacity hinders their applications at commercial level (Shehata et al. 2021; Siyal et al. 2018). In our previous work, PAGP based on metakaolin adsorbed ~ 2 mg/g MB which was very low compared to existing commercial adsorbents, e.g., activated carbon, zeolites, and mesoporous silica (Khan et al. 2015). One of the limitations related to geopolymer adsorbents is the difficulty in beads preparation as they need at least 72 h to cure completely. In some of the previous works, beads are prepared from geopolymer at the early stages of the reaction, e.g., (Papa et al. 2020) fabricated geopolymer beads using ice-templating by dropping the geopolymer paste to liquid nitrogen. In another work, low molecular weight poly ethylene glycol is used as medium to form geopolymer beads (Medri et al. 2020). Dropping geopolymer paste to heated oil, PEG, and liquid nitrogen will stop process of geopolymerization, and a partial geopolymer may be formed as process of geopolymerization require at least 3 days (Provis 2014; Provis and Bernal 2014).

It is proposed that the efficiency of PAGPs can be improved by preparation of hybrid composites with biopolymers and surfactants (Celerier et al. 2018; Cui et al. 2011; Derouiche and Baklouti 2021). Therefore, an approach is needed to use fully cured geopolymers mixed with some biopolymer to affectively remediate pollutants, e.g., methylene blue from wastewater.

The goal of this work is to use hybrid geopolymers beads based on phosphoric acid geopolymer, SLS, and calcium alginate to remove methylene blue from water sample aiming that this combination will enhance MB removal efficiency leading to highly effective adsorbent. The understanding of hybrid materials employed as adsorbents for the removal of MB will be furthered by this work. To the best of our knowledge, it is the first study to use ternary hybrid material based on completely cured phosphoric acid geopolymers, alginate, and SLS. This study will open a new window toward ternary geopolymer composite beads for wastewater treatment. Combination of a green polymer (PAGP) prepared from waste material (fly ash), combined with green bio polymer (alginate) may be an environment friendly material for the wastewater treatment.

## Material and methods

### Materials

Powdered coal fly ash (FA) was obtained from Lumut power plant, Malaysia, and was used without further treatment. According to the X-rays fluorescence (XRF) analysis, FA contains 44.52%  $\text{SiO}_2$ , 22.5%  $\text{Al}_2\text{O}_3$ , 11.6%  $\text{Fe}_2\text{O}_3$ , and 9.84%  $\text{CaO}$  and is termed as class F-fly ash in accordance with ASTM C618 (Pourkhorshidi et al. 2010). Calcium chloride, sodium alginate (SA), sodium lauryl sulfate (SLS), methylene blue, sodium hydroxide, sodium chloride, hydrochloric acid, ethanol, and isopropanol were procured from

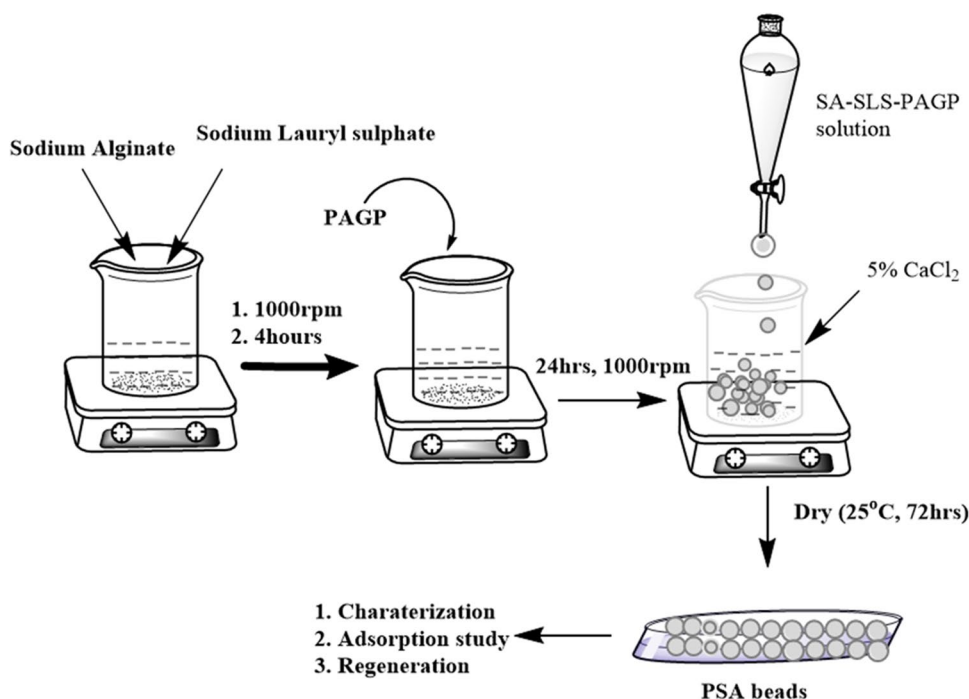
local chemical suppliers. Deionized water was used throughout this work.

### Preparation of PSA beads

Firstly, calcium alginate beads (samples without PAGP and SLS) were prepared by drop-by-drop addition of 2% sodium alginate solution to 5% calcium chloride solution followed by room temperature drying till constant mass. PAGP was prepared using coal fly ash and phosphoric acid with P:AL ratio of 1:1 using methodology reported in our previous work except that metakaolin was replaced by FA (Khan et al. 2015). PAGP-alginate binary composite was prepared by adding 4 g of PAGP to 100 ml of 2% sodium alginate solution followed by drop-by-drop addition to the 5% calcium chloride solution and room temperature drying.

PSA beads were prepared, using methodology depicted in Fig. 1, using PAGP, SA solution, SLS, and  $\text{CaCl}_2$ . In this protocol, 2 g of SA was gradually dissolved in 100 ml of demineralized water with the help of continuous stirring at 1000 rpm. The alginate completely dissolved in 4 h resulting in a transparent solution. Sodium lauryl sulfate (1 g) was introduced into the 2% SA solution, and the mixture was stirred continuously for a duration of 4 h to get homogenous solution followed by addition of 4 g of PAGP powder (it is the maximum amount of PAGP that can be successfully added) prepared using fly ash and phosphoric acid following previously reported protocol (Khan et al. 2015). The sample was stirred using a magnetic stirring hot plate (MSH 20D, Wise stir) for 24 h at 1000 rpm to attain a stable and

**Fig. 1** Methodology for the preparation of PSA beads



uniform suspension. This SA-SLS-PAGP suspension was added dropwise with the aid of a dropping funnel into a 500-ml beaker containing 100 ml of 5% aqueous  $\text{CaCl}_2$  solution. The solution was stirred at 50 rotation per minute (rpm) (higher rpm led to formation of threads), and the formation of PSA beads was witnessed.

The adsorbent beads were allowed to stand in the calcium-rich solution for over night to complete Na-Ca exchange process and then rinsed with demineralized water to eradicate the excess of surfactant and sodium chloride formed in this process. After filtration, the beads were air-dried at room temperature over a period of 3 days, ultimately producing the final adsorbent that was analyzed using SEM, FTIR, BET, XRD, TGA, and PZC analysis and evaluated for adsorption of methylene blue dye.

### Characterization of PSA beads

The PAGP-SLS-alginate beads (PSA beads) were characterized using SEM, FTIR, XRD, TGA, BET, and point zero charge analysis following standard methods reported in the literature (Almas et al. 2022; Ge et al. 2017). For morphology studies, PSA beads were visualized using scanning electron microscope (TESCAN Vega, Czech Republic) after mounting the sample using a carbon tap on the aluminum stub and analyzed at various magnifications (100–3000 $\times$ ) at 10 keV energy. The chemical composition of the PSA beads was determined with the help of energy dispersive X-rays (EDX) function of SEM. FTIR analysis of the PAGP and PSA beads was undertaken using ATR-FTIR (Perkin Elmer, US) in the wavenumber range of 4000 to 450  $\text{cm}^{-1}$ . Existence of crystalline phases and amorphousity was determined using X-ray diffraction analysis in 2-theta range of 2–80°. Surface area analyzer (ASAP 2020, Micromeritics) was employed to inspect the surface profile of the sample using  $\text{N}_2$  adsorption and desorption methods. The thermal stability and degradability of the PSA beads was systematically investigated utilizing simultaneous thermal analyzer (STA 6000, Perkin Elmer). The analysis was conducted under a nitrogen atmosphere, covering a temperature range from 30 to 800 °C, and employing a controlled heating rate of 10 °C

per min. The % mass loss in the form of thermogram (TG) and its derivative as DTG was recorded. To determine the point of zero charge (PZC), electrolyte addition technique, discussed in the previous studies, was used (El-Habacha et al. 2023; Zyoud et al. 2023). This approach makes use of NaCl solution (0.1 M, 50 mL) and adjusting the pH of the NaCl solutions in the range 2 to 10 with the help of HCl (0.1 M) or NaOH (0.1 M) solutions. PSA adsorbent (0.1 g) was added to each flask and shaken for 24 h at 200 rpm using orbital shaker. The concluding pH values of the samples were documented, and the variance between the initial and final pH readings ( $\Delta\text{pH} = \text{pHi} - \text{pHf}$ ) was graphically plotted against initial pH. The intersection of the resultant curve and the pH axis delineates the value corresponding to the point of zero charge (Mosoarca et al. 2020).

### Adsorption study

The variation of MB adsorption by different adsorbents (prepared in this work) was investigated by adding 0.1 g of each adsorbent to 50 ml of a 200 mg/L MB solution followed by shaking at 200 rpm for 300 min. The impacts of pH, dosage of adsorbent, concentration of MB solution, contact duration, and temperature were investigated under different conditions, as outlined in Table 1. To examine the effect of pH, a 50 ml MB solution containing 100  $\text{mg} \cdot \text{L}^{-1}$  of MB and 0.1 g of PSA beads was shaken at 5 different pHs, at 200 rpm in a multifunctional orbital shaker (PSU 20i, Biosan) for 5 h at room temperature. The mixture was then segregated using a mechanical sieve (due to considerable size of the beads, the separation can be achieved) and analyzed using a UV-Vis spectrophotometer (UV-1800, Shimadzu, Japan) in photometric mode. The concentration of MB solution was determined at a fixed wavelength of 664 nm using a single wavelength calibration curve method in the concentration range of 1–25 parts per million ( $\text{mg} \cdot \text{L}^{-1}$ ) (Khan et al. 2015; Mosoarca et al. 2020). To investigate adsorbent dosage's impact, 0.06, 0.08, 0.10, and 0.12 g of PSA beads were added to the MB solution (50 ml, 100  $\text{mg} \cdot \text{L}^{-1}$ ) and shaken for 300 min. To determine the effect of MB concentration, 50 ml MB solutions having concentration in the range of 50–500 mg/L were mechanically shaken with

**Table 1** Parameters used in the studying the influence of different variables on the adsorption of methylene blue (MB) on PSA beads. ( $V = 0.05$  L, rpm = 200 rpm)

	pH	Dosage (g)	Conc (mg/L)	Time (min)	Temp (°C)
Effect of pH	2, 4, 6, 8, 10	0.1	100	300	25
Effect of dosage	7	0.06, 0.08, 0.10, 0.12	100	300	25
Effect of dye conc	7	0.1	50, 100, 200, 300, 400, 500	300	25
Effect of time	7	0.1	100	15, 30, 60, 120, 240, 270, 300	25
Effect of temp	7	0.1	100	300	25, 35, 45

0.1 g of adsorbent for 5 h. The effect of time and temperature was studied by examining the MB adsorption at various time intervals (15 to 300 min) and temperatures (25 °C, 35 °C, and 45 °C) as presented in Table 1. The concentration of MB was determined using UV–Vis spectrophotometer, and the amount of dye adsorbed was calculated using Eqs. 1 and 2.

$$\% \text{ Removal} = \frac{(C_0 - C_f)}{C_0} 100 \tag{1}$$

$$\text{Adsorption capacity } (Q) = \frac{(C_0 - C_f)}{m} V \tag{2}$$

In Eqs. 1 and 2,  $C_0$  and  $C_f$  represent MB concentrations in mg. L<sup>-1</sup> at time  $t=0$  and  $t=\text{maximum time}$ ,  $V$  is volume of MB solution in liters, and  $m$  is mass of PSA beads in grams.

### Kinetics study

Kinetics study is aimed to know the order, speed, and mechanism of a reaction. The data obtained from the adsorption of MB at different time intervals is used for the determination of kinetics parameters. The kinetics of the MB adsorption process was assessed using the Lagergren pseudo-first-order (PFO) and pseudo-second-order (PSO) equations, and the intraparticle diffusion (IPD) and liquid film diffusion (LFD) equations were employed to forecast the diffusion mode in the PSA beads and to predict the adsorption mechanism as well (Lagergren 1898). Equations 3–6 represent the equations used by PFO, PSO, IPD, and LFD models, respectively, and the linear plot of  $\log(Q_e - Q_t)$  vs  $t$  (PFO model),  $t/Q_t$  vs  $t$  (PSO model),  $Q_t$  vs  $t^{1/2}$  (IPD model), and  $\ln(1 - F)$  vs  $t$  (LFD model) were used for calculating various adsorption parameters (Hamdaoui 2006; Revellame et al. 2020; Shen 2008; Wu et al. 2009).

$$\log(Q_e - Q_t) = \log(Q_e) - \frac{K_1 t}{2.303} \tag{3}$$

$$\frac{t}{Q_t} = \left(\frac{1}{Q_e}\right)t - \frac{1}{K_2 Q_e^2} \tag{4}$$

$$Q_t = k_p t^{1/2} + C \tag{5}$$

$$\ln(1 - F) = -k_f t \tag{6}$$

In these equations,  $Q_e$  represents the adsorption capacity at equilibrium, while  $Q_t$  denotes the adsorption capacity at a specific time  $t$ ,  $K$  is constant of the equation,  $t$  is the time interval,  $C$  is IPD model’s intercept, and  $F = Q_t/Q_e$ . The extent of fitting represented by  $R^2$  determines which model fitted well on the kinetics data.

### Adsorption isotherms

Adsorption isotherms define the nature of the adsorption, understanding adsorption capacity, selection of material, the mechanism of the process and design of the process. In this work, four different isotherm models, i.e., Langmuir, Freundlich, Temkin, and Dubinin-Radushkevich (DR) were employed based on Eqs. 7, 8, 9, and 10, respectively.

$$\frac{1}{Q_e} = \frac{1}{Q_m} + \frac{1}{K_L Q_m C_e} \tag{7}$$

$$\log Q_e = \log K_F + \frac{1}{n} \log C_e \tag{8}$$

$$Q_e = B \ln A + B \ln C_e \tag{9}$$

$$\ln Q_e = \ln k - \beta (RT \ln(1 + 1/C))^2 \tag{10}$$

In Eqs. 7, 8, 9, and 10,  $Q_m$  denotes the maximum adsorption capacity,  $K_L$  represents the energy of adsorption obtained from the Langmuir equation, and  $K_F$  and  $n$  are the Freundlich constants indicating adsorption intensity. Additionally,  $B$  signifies the Temkin constant associated with the heat of sorption in joules per mole (J. mol<sup>-1</sup>), while  $A$  corresponds to the Temkin isotherm constant in Liter per gram (L. g<sup>-1</sup>). Lastly,  $\beta$  is a constant related to the mean free energy of adsorption (in k. J<sup>2</sup>. mol<sup>-2</sup>),  $R$  is ideal gas constant, and  $C$  is concentration of MB. For isotherm study, the data obtained in effect of concentration on MB adsorption was used using linear plot of Eqs. 7, 8, 9, and 10, and the best fit ( $R^2$ ) was used as the standard to define which model explains the adsorption process. Another parameter based on Langmuir isotherm is  $R_L$  and it is calculated using Eq. 11.

$$R_L = \frac{1}{(1 + k_L C_0)} \tag{11}$$

The  $R_L$  value based on Langmuir isotherm predicts the nature of adsorption:  $R_L > 1$  shows unfavorable,  $R_L = 1$  for linear, and  $0 < R_L < 1$  for favorable adsorption, whereas  $R_L = 0$  indicates irreversible adsorption with all adsorption sites occupied (Al-Ghouti and Al-Absi 2020).

### Adsorption thermodynamics

The thermodynamics of adsorption is vital because it provides insights into the energy changes taking place during the adsorption and the spontaneity of the process. It helps in understanding the stability and efficiency of adsorption systems, aiding in the design and optimization of adsorption processes for various applications. Additionally,



thermodynamic parameters offer valuable information for predicting equilibrium conditions and assessing the feasibility of adsorption in environmental and industrial applications (Al-Ghouti and Al-Absi 2020; Khan et al. 2013). Equations 12, 13, and 14 were applied to calculate the thermodynamic parameters, including the enthalpy change ( $\Delta H$ ), change in free energy ( $\Delta G$ ), and change in entropy ( $\Delta S$ ).

$$K_c = \frac{Q_e}{C_e} \quad (12)$$

$$\ln(k_c) = \frac{\Delta S}{R} - \frac{\Delta H}{RT} \quad (13)$$

$$\Delta G = \Delta H - T\Delta S \quad (14)$$

### Desorption study and re-usability

Desorption study is an important part of MB adsorption study to ensure continuous use of the adsorbent. Ethanol, isopropanol, 1 N NaOH, and 1 N HCl solution were used for regeneration of PSA beads. Initially, 0.1 g of the spent adsorbent (prepared by adsorbing a 200 mg/L MB solution on 0.1 g of adsorbent) was stirred with 50 ml of each solvent in an

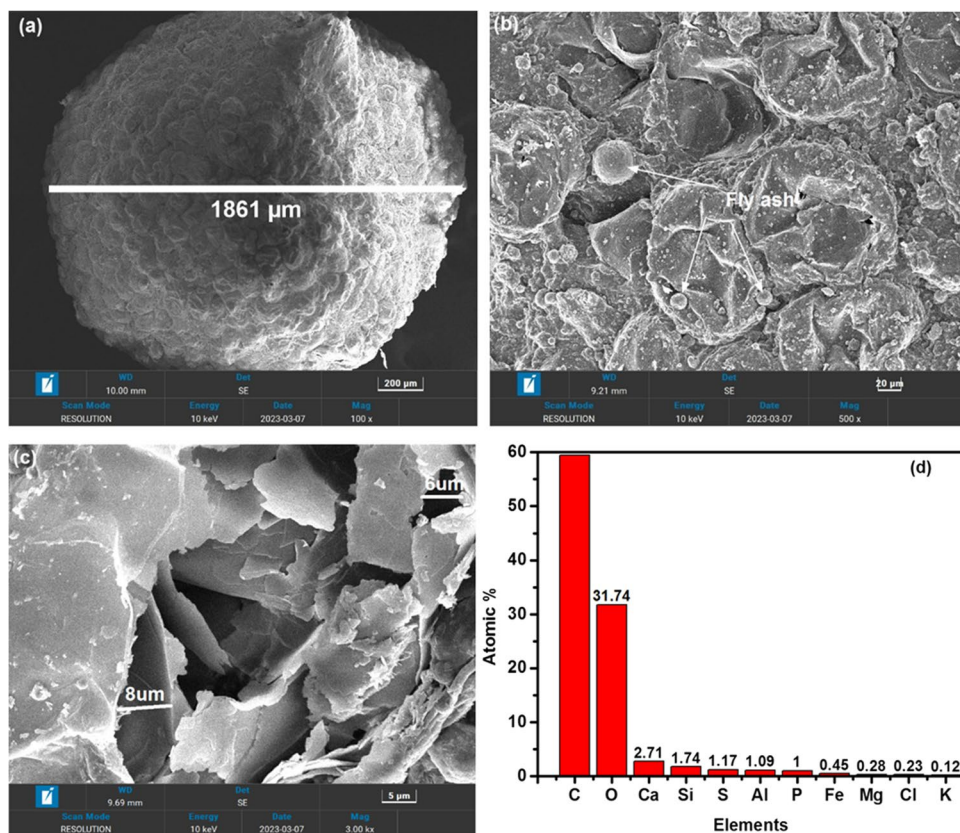
orbital mixer at 200 rpm for 2 h. The amount of desorbed dye was determined using a UV–Vis spectrophotometer, and the % recovery and desorption capacities were calculated using Eqs. 1 and 2. The desorbed PSA beads were dried and subsequently reused for methylene blue (MB) adsorption over five cycles, employing 100mg/L MB solution, 0.1 g of adsorbent, and 50 ml of dye solution.

## Results and discussions

### Adsorbent's characterization

SEM (scanning electron microscopy) provides microscopic-level information about the microstructure of materials, facilitating a deeper understanding and strengthening correlations between various factors and the microscopic properties and activities of the material. Figure 2(a, b, and c) illustrates the SEM micrographs of PSA beads at various resolutions, with a more detailed view impeded by the onset of backscattering beyond that resolution. Figure 2a depicts micrograph of a single PSA bead at 100 times magnification, and the size of PSA beads is observed to be 1861  $\mu\text{m}$ . The surface is smooth with slight roughness and showing the presence of geopolymer (agglomerates) and fly ash spheres (unreacted FA). PAGP particles and plates, unreacted fly ash,

**Fig. 2** a–c SEM micrographs of PAGP-alginate hybrid beads from various points at various magnifications. **d** EDX analysis of PSA beads



and cracks are witnessed clearly in Fig. 2b (image at 500 $\times$ ). On further zooming the sample, micron sized voids were observed as shown in Fig. 2c (image at 3 k $\times$ ). Moreover, plate-like morphologies were found in the micrograph presented in Fig. 2c. The EDX analysis is depicted in Fig. 2d, representing that carbon and oxygen are major components of the PSA beads. Additionally, Ca, Si, S, Al, P, Fe, Mg, Cl, and K were observed in the EDX analysis of PSA beads.

The micrographs depict that PSA beads have smooth surface representing good homogeneity between calcium alginate and PAGPs. The absence of large cracks on the surface of the beads further supports the compatibility of biopolymers and PAGP. Porous surface made up of plates-like morphologies of varying sizes are produced due to release of water molecules during drying (Kondaveeti et al. 2022; Liu et al. 2016; Tanimoto et al. 2023). Size of the pores are macro porous having size in the range of 1–10  $\mu\text{m}$ . The plates seem to be geopolymer embedded in the alginate matrix. Existence of unreacted or partially reacted fly ash particles explains that during PAGP formation, all fly ash did not react completely due to the presence of crystalline quartzite phase in FA (Prabhakar et al. 2023).

The SEM images of the PSA are slightly different than those reported in the previous works owing to the extended mixing time and presence of surfactants in the samples; the geopolymer particles unglued from each other and acquired the profile of irregular plates (Almas et al. 2022; Ge et al. 2017; Provis and Bernal 2014). The unreacted or partially reacted fly ash particle, mostly observed in fly ash-based geopolymers, has broken down into tiny particles due to the leaching effect of phosphoric acid. As the PSA beads were dried at room temperature over a period of 3 days, therefore, the release of water molecules may caused the formation of voids/pores on the surface of PSA beads. In the EDX analysis, C and O content is related to the carbon tap used for holding samples and organic backbone of alginate and SLS, whereas other elements are linked with silico alumino phosphate network of PAGP (Khan et al. 2015). The absence of sodium witnessed the conversion of all sodium alginate to calcium alginate (Lotfy et al. 2023). The P:Al ratio of 1:1 is also established by the EDX analysis.

Figure 3 represents the FTIR analysis of the PSA beads and PAGP samples using ATR-FTIR technique. The spectra are consisted of visible and notable absorption frequencies at 3433, 2963, 2916, 2847, 1620, 1466, 1423, 1251, 1218, 1102, 961, and 627  $\text{cm}^{-1}$ . In FTIR spectrum of the PSA beads, the frequency band at 3433  $\text{cm}^{-1}$  corresponds to the existence of hydroxyl ( $-\text{OH}$ ) group, while characteristic peaks at 2963  $\text{cm}^{-1}$ , 2916  $\text{cm}^{-1}$ , and 2844  $\text{cm}^{-1}$  specify C–H bonds in alginate and SLS (Ge et al. 2017). Frequency bands at 1620, 1466, and 1423  $\text{cm}^{-1}$  are produced by the carboxylic C=O (Asy. and sym, stretching vibrations) of the alginate molecule. Furthermore, the bands at 1251 and 1218

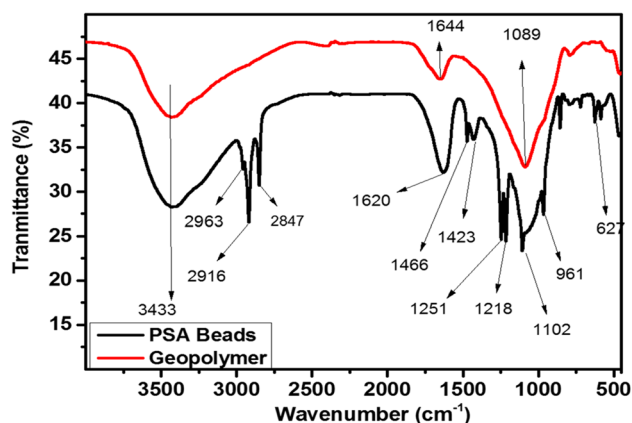


Fig. 3 FTIR analysis of PAGP and PSA beads

$\text{cm}^{-1}$  can be attributed to the C–O and C–C stretching vibrations within the ring, and those at 1102  $\text{cm}^{-1}$  can be assigned to C–OH, Si–O, Al–O, and P–O groups. Lastly, the peak at 627  $\text{cm}^{-1}$  is produced by the Ca–O bond formed from the crosslinking of Ca and alginate chains (Lotfy et al. 2023). In PAGP spectrum, peaks at 3433, 1644, and 1089  $\text{cm}^{-1}$  represent the O–H, and M–O bonds (M represents Si, Al, or P). The frequency band at 1089  $\text{cm}^{-1}$  is a typical peak observed in PAGPs due to the formation of O–Al–O–P–O–Si– type bonds (Khan et al. 2015). The spectra closely resemble with the FTIR spectrum of PAGP and geopolymers-alginate beads reported in previous studies (Celerier et al. 2018; Ge et al. 2017; Khan et al. 2015).

Figure 4 describes the powder X-rays diffraction analysis of the PAGP and PSA beads in the 2-theta range of 2–80°. A closer examination of the XRD analysis describes that both samples are amorphous in nature with few crystalline phases. The PAGP diffractogram is very simple and has only few bands in the 2-theta range of 15 to 40°. As given in Fig. 4, the PAGP diffractogram has a broad hump in the

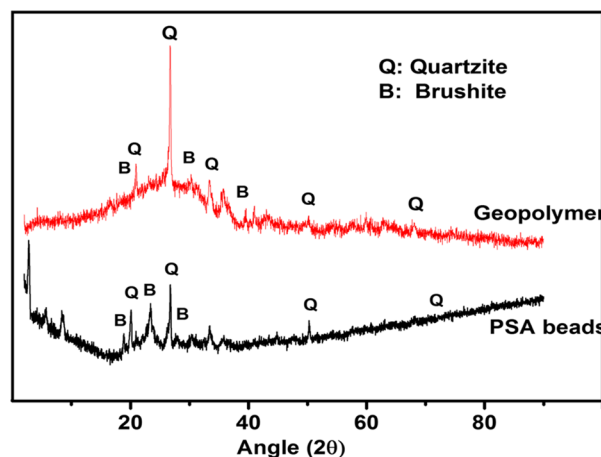


Fig. 4 XRD analysis of the PAGP and PSA beads

range of 22 to 26°, representing the amorphous nature of the sample (Khan et al. 2015). In addition to the amorphous material, the presence of the quartzite phase is indicated by the pattern observed at 20.78°, 26.61°, 50.25°, 60.03°, and 68.28° (Otzen et al. 2023). Mullite and brushite phases are witnessed in both PAGP and PSA beads samples. The quartzite, mullite, and brushite phases are produced by fly ash and PAGP, whereas CA has no crystallinity. By comparing Fig. 4 with the literature, it is concluded that the PAGP sample represents the typical XRD diffractogram of the geopolymers prepared by H<sub>3</sub>PO<sub>4</sub> activation of fly ash (Celerier et al. 2018; Khan et al. 2015). Similar with the PAGP diffractogram, the PSA beads diffractogram also shows the same characteristics pattern.

Figure 5 illustrates the nitrogen adsorption–desorption isotherm obtained through BET surface area and porosimetry analysis, revealing that the PSA beads showcase a BET surface area of 1.97 m<sup>2</sup>/g, BET adsorption pore diameter of 6.42 nm, and cumulative pore volume of 0.003038 cm<sup>3</sup>/g (determined by BJH adsorption within the pore size range of 1.700 to 300 nm). During desorption, the BJH desorption cumulative volume of pores within the diameter range of 1.7 to 300 nm is determined to be 0.003742 cm<sup>3</sup>/g. The isotherm, depicting relative pressure versus the quantity adsorbed, exhibits a hysteresis loop characteristic of a type IV isotherm according to the IUPAC classification (Thommes et al. 2015). The results demonstrated that mesoporous adsorbent (PSA beads) is being formed by the combination of geopolymer, SLS, and Ca-alginate.

Figure 6 displays the TGA analysis of the PSA beads, performed under a nitrogen atmosphere with the heating rate of 10 °C/min, covering the temperature range of 25 to 800 °C. A total of 35% mass loss is observed in the three visible steps, i.e., 25–200 °C, 200–250 °C, and 540–600 °C. The first step is a slower mass loss, followed by a steeper mass abatement (that contributed for most of the mass depletion), and the last step contributed for only up to 5% of the

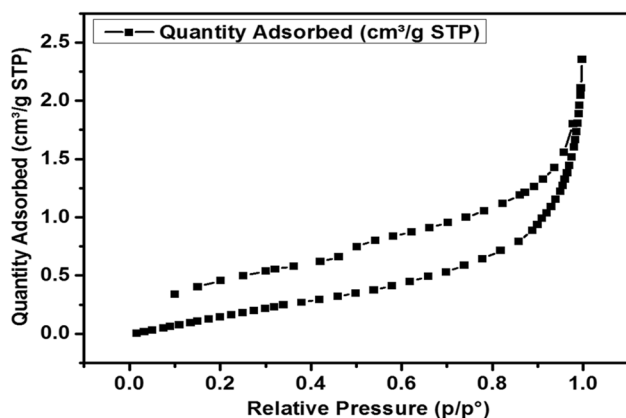


Fig. 5 BET isotherm results of PSA beads

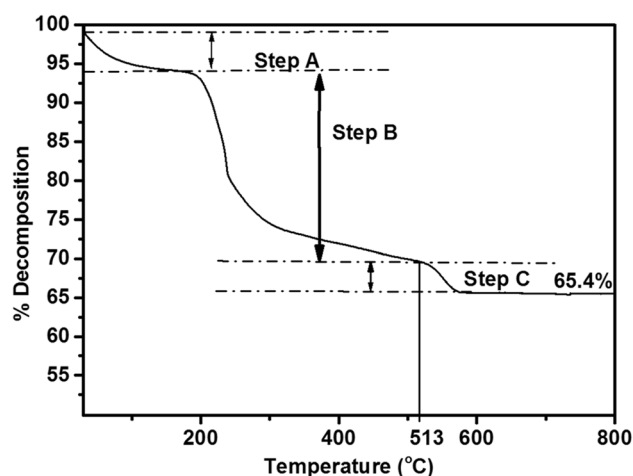


Fig. 6 TGA analysis of PSA beads under nitrogen environment

mass loss. The evaporation of water molecules trapped on the surface, and inside the PSA beads is represented by the first step of mass loss (Kondaveeti et al. 2022). The passive vaporization evidenced by the less steep TGA curve represents that water molecules are released from various points, e.g., surface, inside, and even from the geopolymer matrix as well. The second and third steps represent the pyrolysis of calcium alginate structure (Ahmad et al. 2023).

The PZC analysis of the PSA beads is depicted in Fig. 7, and the measured  $\text{pH}_{\text{pzc}}$  value is 7.448 computed by employing the average of the points that remained constant for the final pH. At this specific pH level, the positive surface sites attain a charge equilibrium with the negative ones, resulting in a neutral surface charge (zero charge). This parameter holds significance as it facilitates the evaluation of the pH's influence on the adsorption process by forecasting the adsorbent surface charge relative to pH. In a solution, the sorbent

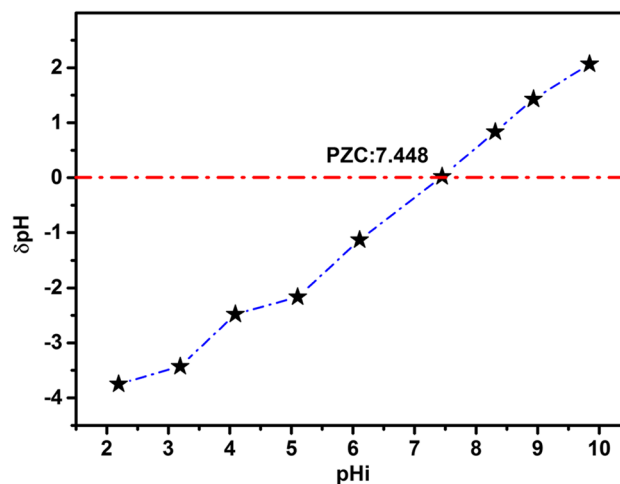


Fig. 7 pHpzc Analysis of the PSA beads using pH method



surface carries a negative charge, allowing interaction with positive species when pH exceeds  $pH_{pzc}$ . Conversely, when the pH is below  $pH_{pzc}$ , the solid surface acquires a positive charge, enabling interaction with negative species (Yasir et al. 2022).

## Adsorption study

### Effect of type of adsorbent

Figure 8 represents the adsorption capacity of four different adsorbents for 200 mg/L MB solution at pH7 for 300 min. Calcium alginate beads prepared using ionotropic gelation of sodium alginate and calcium chloride adsorbed 32.35 mg/g which was lowest among the four adsorbents. The MB adsorbed by PAGP, alginate-PAGP binary composite, and PSA beads were 45.13, 55.50, and 95.82 mg/g, respectively. It is evident that the highest remediation of MB is achieved by PSA beads followed Alg-PAGP, PAGP, and alginate beads.

The experimental findings indicate an obvious trend in the methylene blue's adsorption capability across various adsorbents compositions. Notably, the largest adsorption capacity within the compositions investigated was demonstrated by the PSA beads, which showed the highest affinity for MB. Subsequently, the alginate-geopolymer binary composite demonstrated a noteworthy adsorption capacity though lower than PSA beads. The geopolymer beads, on the other hand, showed a reduced adsorption capacity, suggesting a weaker affinity for the methylene dye in comparison to the composite structures. Finally, among the compositions studied, the alginate beads showed the least potential for MB's adsorption. These results highlight how alginate, geopolymer, and SLS work synergistically, and they point to the possible uses in adsorption-based procedures like the

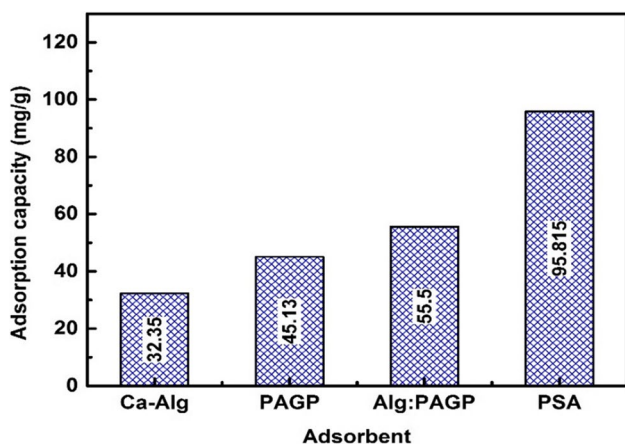


**Fig. 8** Effect of combination of PAGP, Alg, and SLS on adsorption of MB

treatment of wastewater or the elimination of dye from aqueous solutions.

### Effect of pH

The effect of pH on adsorption of MB in terms of % removal and adsorption capacity on PSA beads is presented in Fig. 9. It is evident in the figure that almost above 95.15–96.65% MB removal is achieved at acidic, neutral, and alkaline pHs. Necessary to mention is that final pH of all samples after 5 h of shaking was in the range of pH6 to pH8 representing that PSA beads normalized the pH to neutral pH. The acidic samples attained the final pHs in the range of 6–7.5, and the basic sample resulted into pH 7–8 depending on the initial pH of the samples. The adsorption capacity has shown a slight variation as a function of pH and remained in the range of 47–48.33 mg/g establishing that adsorbent is equally effective at acidic and alkaline pHs. The maximum adsorption capacity was achieved at pH 6–10, i.e., pH close to neutral pH of 7. This behavior of the PSA beads is explained based on the presence of phosphate species in the geopolymer. Phosphoric acid-based geopolymers are made up of repeating  $SiO_4$ ,  $AlO_4$ , and  $PO_4$  units covalently linked via bridging oxygen atoms (Derouiche and Baklouti 2021). PAGPs are considered as neutral geopolymers compared to alkaline and alkali-activated geopolymers. The phosphate species are used as buffers that maintain the pH of the solution. Here, PAGP has played a buffering role by shifting the pH of the MB solution to neutral values (Gameiro et al. 2021). The results demonstrate that PSA beads are effective at all pHs and can be effectively used in acidic, neutral, and basic environments. As the adsorption of the PSA beads is almost same at all pHs, therefore, adsorption study will be conducted at normal pH of the MB solution.

Two important factors to be determined in adsorption studies are adsorbent dosage and adsorbate concentrations.

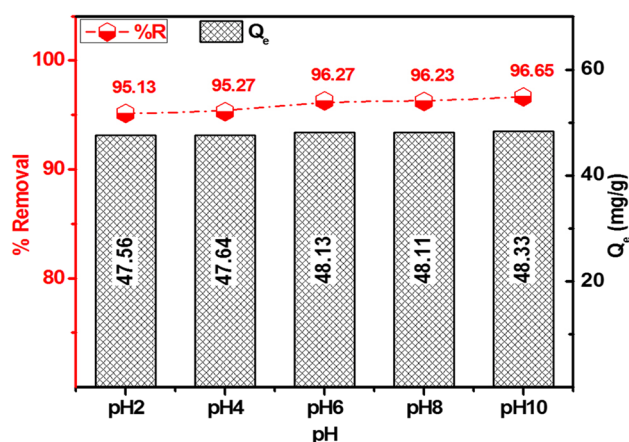


**Fig. 9** Effect of pH on MB adsorption on PSA beads

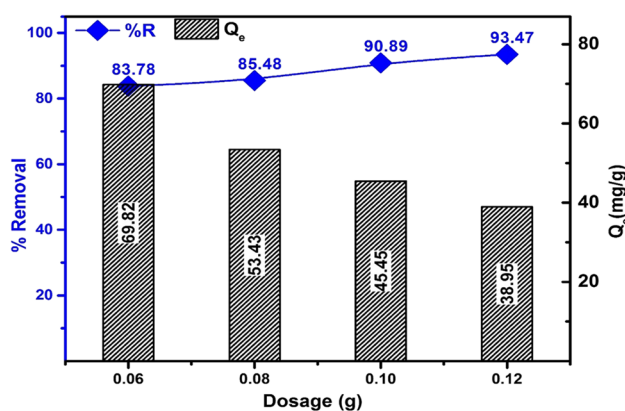


Fig. 10 Impact of adsorbent dosage on MB adsorption PSA beads

Figure 10 shows the per cent removal and adsorption capacity of the MB as a function of adsorbent dosage at a fixed MB concentration and volume. The results reveal that 83.78 to 93.47% of MB was adsorbed by the PSA beads and with the increase of adsorbent amount, a slight increase in adsorption of MB is observed. There is a slight difference between the adsorptive removal of MB at 0.1-g and 0.12-g dosages, i.e., 90.9 vs 93.47%. A decreasing trend is witnessed in the adsorption capacity of PSA at various adsorbent dosages. Maximum adsorption capacity of 69.82 mg. g<sup>-1</sup> was attained at adsorption dosage of 0.06 g. As the adsorption by both 0.1 g and 0.12 g are nearly identical, therefore, adsorbent dosage of 0.1 g was used in further studies being convenient in experimentation. Moreover, 0.1 g adsorbed more than 90% of the MB dye. The rise in methylene blue adsorption (% removal) with an increased adsorbent dosage is attributed to the enhanced availability of active sites on the adsorbent material. As the dosage is elevated, a larger number of adsorbent particles are introduced, providing additional binding sites for the effective capture and retention of methylene blue molecules. This intensified concentration of active sites improves the overall adsorption capacity, leading to a more pronounced removal of methylene blue from the solution. This correlation highlights the direct influence of adsorbent dosage on the efficiency of methylene blue adsorption, emphasizing its pivotal role in optimizing the adsorption process. The decline in adsorption capacity with an increase in adsorbent dosage indicates that 0.06 g of PSA has reached its maximum adsorption capacity for MB, with further increments in adsorbent dosage yielding minimal additional adsorption (Candamano et al. 2023; Ge et al. 2017).

Figure 11 is the graphic presentation of the effect of MB concentration on % removal and adsorption capacity of PSA beads. It is demonstrated that removal efficiency of PSA beads was 97.11%, 97.80%, and 96.38%, 97.06%, 97.39%, and 96.70% for 50 mg/L, 100 mg/L, 200 mg/L, 300 mg/L, 400 mg/L, and 500 mg/L MB solution, respectively.

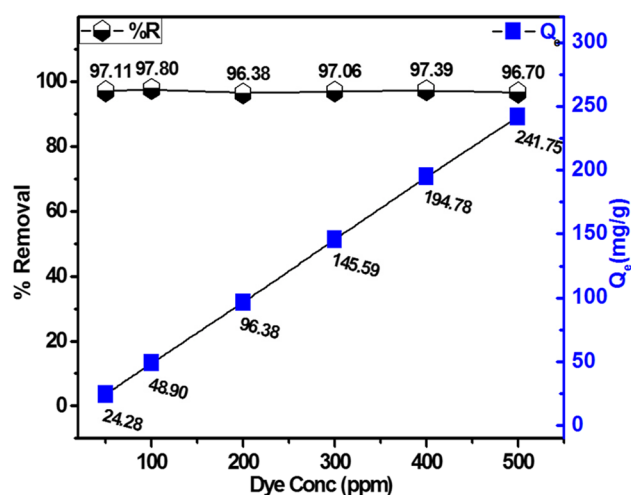


Fig. 11 The effect of dye concentration on MB removal using PSA beads

400 mg/L, and 500 mg/L, respectively. On the other side, the adsorption capacity recorded was 24.28 mg. g<sup>-1</sup>, 48.90 mg. g<sup>-1</sup>, 96.38 mg. g<sup>-1</sup>, 145.59 mg. g<sup>-1</sup>, 194.78 mg. g<sup>-1</sup>, and 241.75 mg. g<sup>-1</sup> for 50 mg/L, 100 mg/L, 200 mg/L, 300 mg/L, 400 mg/L, and 500 mg/L MB solution, respectively. A constant tendency in terms of %removal and an increasing trend in terms of adsorption capacity is observed, in this study.

The variation in % removal owing to changing MB concentration is linked with the effect of increasing MB concentration and enhanced dye remediation ability of the adsorbent. The higher adsorption capacity at higher MB concentration is associated with driving force created by the higher concentration of MB that forces the MB into the PSA beads. It is also assumed that interaction between MB molecules is surpassed by the interaction between MB and PSA beads (Almas et al. 2022; Khan et al. 2015). Moreover, it also signifies the higher adsorption of MB using PSA beads.

### Effect of time and temperature

The role of time and temperature is required to study kinetics and thermodynamics of the adsorption process. Figure 12 is the illustrative demonstration of the MB adsorption by PSA beads over a time interval of 300 min. A fast adsorption is observed in the start leading to 85.8% and 92.6% removal in first 15 and 30 min. In the next 270 min, the % adsorption increased to 98.1% showing an 12% increase for the total 270 min of shaking. The adsorption capacity also abruptly increased in the first 30 min and then a minor variation is witnessed.

It is concluded that equilibrium has attained in 270–300 min of time. This time is quite good compared to 2400 min reported previously for alumino silicate geopolymer-alginate

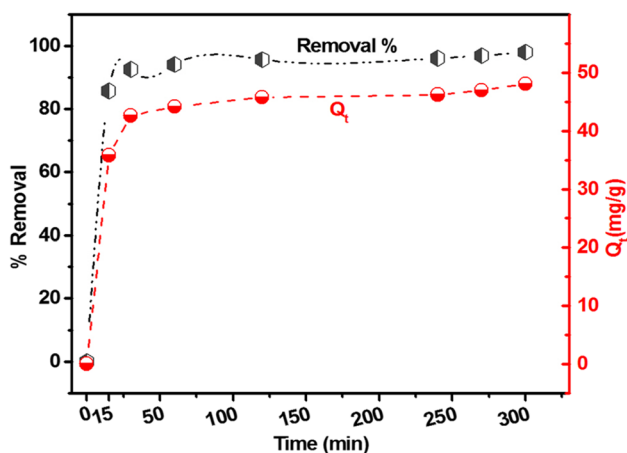
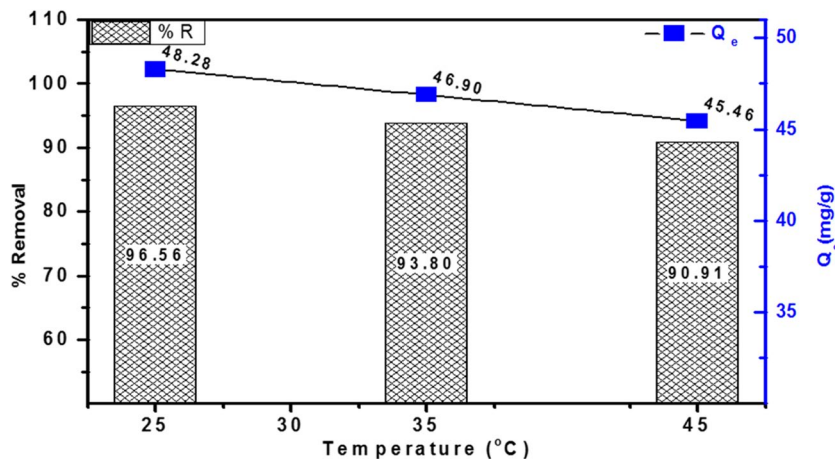


Fig. 12 Effect of time on the adsorption of MB on PSA beads at  $C_i = 100$  mg/L

beads (Ge et al. 2017; Novais et al. 2019). This reduction in time may be linked with the addition of SLS to the geopolymer system that reduced the surface tension of the alginate encapsulation. SLS is an anionic surfactant and helps in increasing the adsorption of cationic dyes, e.g., methylene blue (Almas et al. 2022). Initially, there is a swift rise in the adsorption capacity due to the elevated likelihood of methylene blue (MB) molecules taking up positions on the sites within the hydrogel beads and the surplus available active sites. As time progresses, the adsorption sites become filled, resulting in a reduced probability of interaction between MB and these sites. Consequently, the pace of adsorption progressively decelerates until reaching a state of equilibrium (Almas et al. 2022).

The impact of temperature on adsorptive removal of MB with the help of PSA beads is depicted in Fig. 13. It is very prominent in Fig. 13 that with the increase in temperature from 25 to 35 and 45 °C, there is a decreasing trend of the MB adsorption. 96.56%, 93.80%, and 90.91% of MB was

Fig. 13 Effect of temperature on adsorption of methylene blue



adsorbed at 25 °C, 35 °C, and 45 °C, respectively. Like % removal, adsorption capacity of the PSA beads presented a decreasing pattern with elevation in the temperature. The results indicate that exothermic adsorption occurs, which decreases with an increase in temperature (Salvestrini et al. 2022). Furthermore, at elevated temperatures, increased thermal energy disrupts the adsorption–desorption equilibrium, leading to a higher rate of methylene blue desorption from the adsorbent surface. The enhanced thermal motion weakens the attractive forces between the adsorbent and methylene blue molecules, reducing the overall adsorption capacity. Additionally, high temperatures can induce molecular changes in both the adsorbent and methylene blue, further influencing their interaction (Khapre et al. 2022). A similar trend has been reported in geopolymer-based adsorbent for MB removal (Khan et al. 2015; Nurddin et al. 2020; Siyal et al. 2018).

**Isotherm study**

The adsorption isotherms forecast whether and how the molecules of the adsorbate will interact with those of the adsorbent and reveal the details about the types of interactions. For determining the adsorption capacity at equilibrium and other adsorption-related parameters, 36 different types of adsorption isotherms have been developed (Mozaffar Majd et al. 2022). In this work, four well known isotherms, i.e., Langmuir, Freundlich, Temkin, and D-R isotherms are used. Figure 14(a, b, c, and d) represents the Langmuir, Freundlich, Temkin, and D-R isotherm plots (based on Eqs. 7, 8, 9, and 10) for adsorption of methylene blue on PSA beads. The concentration vs adsorption capacity data is plotted, and the best isotherm is found using degree of fitness ( $R^2$ ) of the linear fit of the experimental data. The calculated parameters based on Eqs. 7, 8, 9, and 10 are tabulated in the form of Table 2, and Langmuir isotherm fitted well compared to Freundlich, Temkin, and D-R isotherms. Langmuir isotherm

**Fig. 14** Isotherm study of MB adsorption using PSA beads. **a** Langmuir isotherm. **b** Freundlich isotherm. **c** Temkin isotherm. **d** DR isotherm **d**  $R_L$  vs  $C_e$

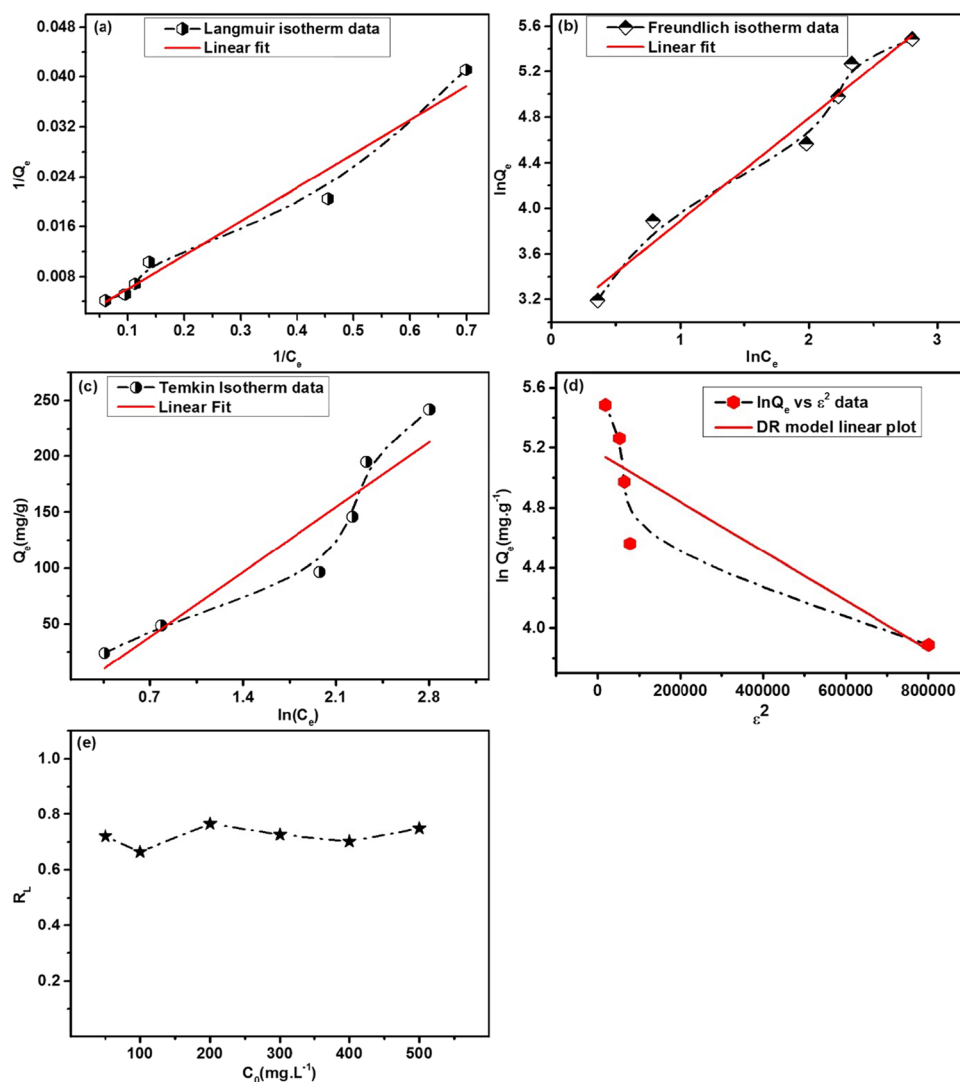


**Table 2** Isotherm data obtained from conc vs adsorption capacity plots using Langmuir, Freundlich, and Temkin isotherms given in Fig. 13

Isotherm	Parameters	Values
Langmuir	$Q_m$ (mg. g <sup>-1</sup> )	1666.66
	$K_L$ (L. mg <sup>-1</sup> )	0.0077
	$R^2$	0.979
Freundlich	$K_F$ (mg <sup>(1-n)</sup> .L <sup>n</sup> .g <sup>-1</sup> )	18.993
	$n$	1.0824
	$R^2$	0.974
Temkin	A (L. g <sup>-1</sup> )	0.686
	B (J. mol <sup>-1</sup> )	44.294
	$R^2$	0.888
D-R isotherm	$Q_s$ (mg. g <sup>-1</sup> )	167.50
	$R^2$	0.884

resulted in  $Q_m$ ,  $K_L$ , and  $R^2$  values of 1666.67 mg. g<sup>-1</sup>, 0.0077 L. mg<sup>-1</sup>, and 0.979, respectively. The degree of fitting ( $R^2$ ) produced by the linear fit of Freundlich, Temkin, and D-R isotherm were 0.974, 0.884, and 0.888, respectively. It is assumed, in Langmuir isotherm, that the adsorption is taking place on the homogeneous sites of the surface of adsorbent material resulting in monolayer adsorption process. Additionally, it is also assumed that adsorption and desorption processes are reversible. The best fitting of Langmuir isotherm of MB adsorption on PSA beads shows that PSA beads have homogenous sites where all adsorption sites have similar energy (Almas et al. 2022; Candamano et al. 2023; Khan et al. 2015). Moreover, the nature of interaction is chemisorption based on interactions between cationic dye (MB) and phosphoric acid-based geopolymers, alginate, and lauryl sulfate anions. PAGPS have polar Al–O, Si–O, and P–O bonds with the oxygen having partial negative charge. This partial negative charge and oxygen's lone pairs interacts with MB dye. Similar findings regarding MB adsorption on



geopolymers and alginates were observed in some previous studies, as well (Almas et al. 2022; Khan et al. 2015).

It is worth mentioning that the value of  $n$  obtained using the Freundlich isotherm is 1.08, which exceeds 1. In Freundlich isotherm,  $n$  value gives very important insight about the favorability of the adsorption process and the nature of adsorption. If  $n = 1$ , there is a linear adsorption with uniform adsorption process; on the other hand,  $n > 1$  represents that with an increasing concentration of the MB in the solution, the adsorption capacity of the adsorbent experiences a more pronounced rise (Kumar and Tamilarasan 2013). This behavior is commonly linked with the robust interactions between the adsorbate and adsorbent, as well as the occurrence of multilayer adsorption. Moreover, it also supports that chemisorption and multilayer adsorption is taking place. Whereas,  $n < 1$  and  $n = 0$  represents unfavorable and reversible adsorption processes (Khan et al. 2013).

Figure 14(e) represents the variation of the separation factor ( $R_L$ ) with dye's initial concentration, calculated using Eq. 11. An  $R_L$  value between 0 and 1 is indicative of favorable adsorption, where the degree of favorability increases as the  $R_L$  value approaches 0 (Kumar and Tamilarasan 2013). PSA beads exhibit  $R_L$  values ranging from 0.720 to 0.748, indicating that the adsorption of MB on the PSA surface is undeniably favorable. The lower end of the range i.e., 0.720 suggests a higher degree of favorability, while the upper end

of 0.748 indicates favorable adsorption but with a slightly lesser degree (Kumar and Tamilarasan 2013).

### Kinetics study

Adsorption kinetics study is important because it offers insights about the process of adsorption, the effectiveness of that process, and their potential applications in industry. In this study, Lagergren pseudo-first-order, and pseudo-second-order models were used, and the results are plotted in Fig. 15(a and b) (Lagergren 1898). The validity of the models was established using extent of fitting ( $R^2$ ) of the linear fit of the data. As evident in Fig. 15b and Table 3, PSO model fitted well with  $R^2$  of 0.999, whereas PFO model's  $R^2$  is 0.833. Besides the high  $R^2$ , the calculated adsorption capacity using PSO (48.076 mg. g<sup>-1</sup>) closely agreed with experimental  $Q_e$  (48.902 mg. g<sup>-1</sup>). The observation that the adsorption of methylene blue on PSA beads follows the PSO kinetics model signifies that the adsorption process is likely driven by chemisorption, indicating strong interactions between the MB and PSA beads. Moreover, it implies that the rate-limiting step of the adsorption process involves the interaction between the MB and PSA beads, with the assumption that the MB binds chemically to the adsorbent surface (Aouan et al. 2023; Khan et al. 2015).

**Fig. 15** Kinetics study of MB on PSA beads. **a** PFO model. **b** PSO model. **c** IPD model. **d** LFD model

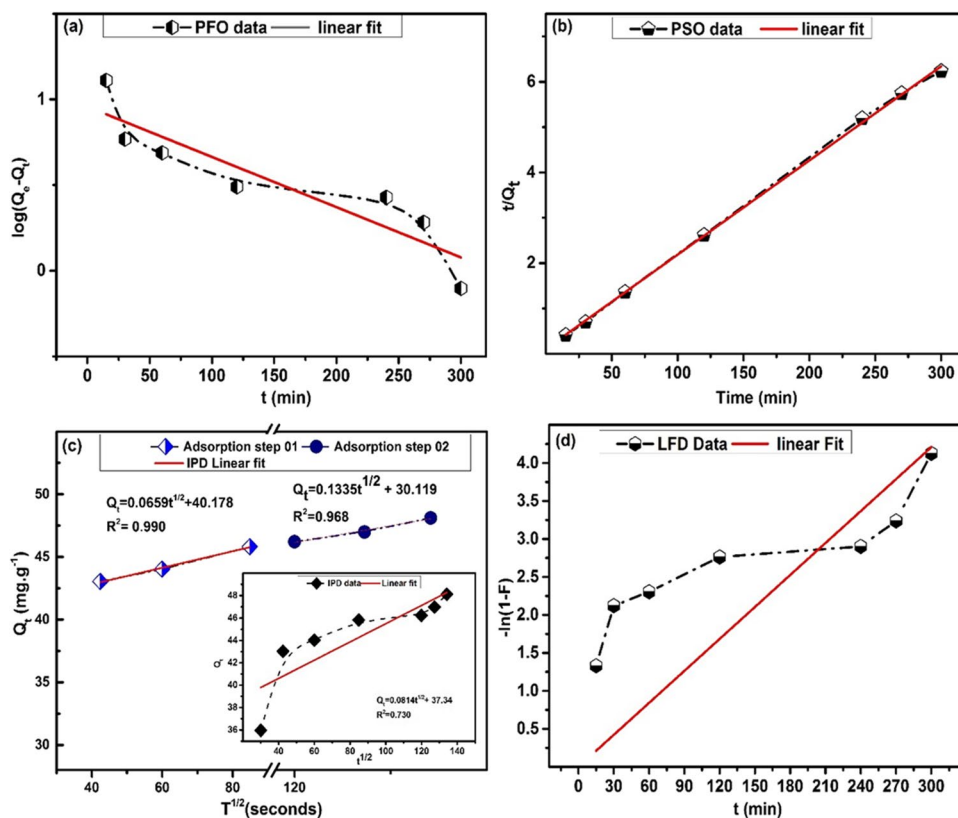


**Table 3** Kinetics study's data obtained from MB adsorption by PSA beads

	$Q$ (mg. g <sup>-1</sup> )	$Q_{e, Cal}$ (mg. g <sup>-1</sup> )	$k_{1(PFO)}$ (min <sup>-1</sup> )	$k_{2(PSO)}$ (min <sup>-1</sup> )	$k_{IPD}$ (mg. g <sup>-1</sup> s <sup>-1/2</sup> )	$k_{LFD}$ (mg. g <sup>-1</sup> min <sup>-1</sup> )	$R^2$
PFO	48.902	2.60	0.0066				0.833
PSO	48.902	48.076		0.0039			0.999
IPD step 01	48.902				0.0659	40.178	0.990
IPD step 02	48.902				0.1335	30.119	
LFD	48.902					0.0140	0.831

As discussed earlier, the PSA beads have SLS, PAGP, and alginate structures, and they interact with cationic methylene blue molecules stabilizing its charges. It is assumed that chemisorption in MB-PSA system is a combination of following types of interactions.

- Interaction between MB and tetrahedral AlO<sub>4</sub>, SiO<sub>4</sub>, and PO<sub>4</sub> units of PAGP (Khan et al. 2015).
- Ion exchange between MB cation and anionic part of SLS.
- Physical interactions between MB cation and Ca-alginate
- Hydrogen bonding between nitrogen atoms of MB and surface silanol, aluminol groups (Aouan et al. 2023; Candamano et al. 2023; Khan et al. 2015; Siyal et al. 2018)

Owing to the multiple interactions, more MB is removed by PSA beads despite their lower surface area. The findings of the present study agree with previously reported literature of MB adsorption on geopolymers as PSO model kinetics is followed by MB adsorption on geopolymers (Aouan et al. 2023; Khan et al. 2015; Siyal et al. 2018). Alkali-activated geopolymers and PAGPs both followed PSO model kinetics with  $R^2$  values of 0.99. Similarly, alginate beads-based adsorbents used for MB adsorption also adopted PSO kinetics (Al-Ghouti and Al-Absi 2020, Liu et al. 2016).

Intraparticle diffusion model and liquid film diffusion models are given in Fig. 15c and d, respectively. Single fitting IPD model (in the in plot) produced a linear fit of  $R^2 = 0.703$  when IPD model was applied on the whole data, representing that single step IPD model is not followed by PSA-MB system. Intraparticle diffusion was not the primary rate-limiting process as  $q_t$  against  $t^{1/2}$  did not pass through (0, 0) as postulated by many researchers (Mosoarca et al. 2020; Wang and Guo 2022; Zhuo et al. 2022). A two-stage IPD fitting, given in Fig. 15c, clearly demonstrates that adsorption process has taken place in two steps, the first step is faster with  $R^2$  of 0.990 and  $K_{IPD}$  value of 0.0659 mg. g<sup>-1</sup>.s<sup>-1/2</sup>. The second is having lower  $R^2$  of 0.968 and interparticle diffusion rate of 0.1335 mg. g<sup>-1</sup>.s<sup>-1/2</sup>. The thickness of the boundary layer is indicated by the intercept value of the IPD

model; the larger the intercept value, the more significant is the boundary layer's impact (El-Ashtoukhy et al. 2008). It is concluded that two-step-IPD is a dominant mechanism in this adsorption process (Kumar and Tamilarasan 2013; Mohamed et al. 2022; Wang and Guo 2022; Zhuo et al. 2022). Liquid film deposition model is described in Fig. 15d, and the data obtained is given in Table 3. The extent of fitting indicated by  $R^2$  (0.831) confirms that LFD mechanism is not dominantly followed.

### Thermodynamics study

Thermodynamics study of the adsorption processes sheds a spotlight on the fundamental forces and mechanisms that control the interaction of the adsorbate molecules with adsorbent surfaces. An in-depth understanding of the driving forces behind adsorption can be captured through a thermodynamic lens, enabling us to interpret equilibrium dynamics.  $K_c$  calculated using Eq. 12 was plotted against the temperature and is presented in Fig. 16, and the thermodynamics parameters, i.e.,  $\Delta H$ ,  $\Delta G$ , and  $\Delta S$  were obtained using Eqs. 13 and 14 (Table 4).

The values obtained for change in enthalpy, Gibbs free energy, and entropy of the adsorption system are  $-40.747$

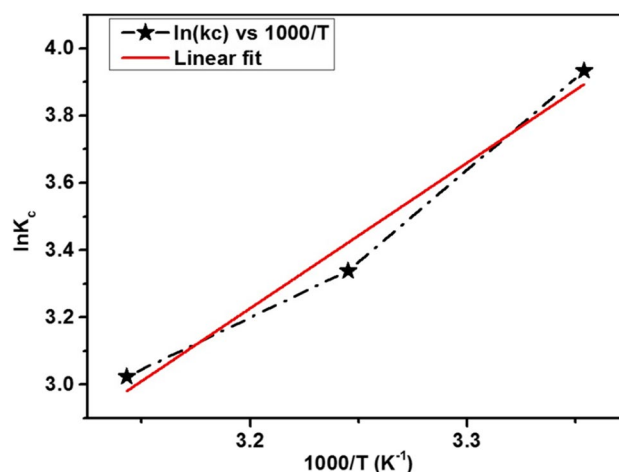


**Fig. 16** The plot of linear correlation between the van't Hoff equation and temperature used for the adsorption of MB-dye on PSA beads

**Table 4** Thermodynamics parameters obtained in this study

T (°C)	$\Delta H$ (kJ. mol <sup>-1</sup> )	$\Delta G$ (kJ. mol <sup>-1</sup> )	$\Delta S$ (J. mol <sup>-1</sup> K <sup>-1</sup> )	R <sup>2</sup>
25	-40.747	-8.198	-109.171	0.990
35		-7.106		0.990
45		-6.014		0.990

kJ. mol<sup>-1</sup>, -8.198 to -6.014 kJ. mol<sup>-1</sup>, and -109.171 J. mol<sup>-1</sup>K<sup>-1</sup>. The change in enthalpy ( $\Delta H$ ) is negative, indicating an exothermic adsorption process. The change in Gibbs free energy ( $\Delta G$ ) also displays a negative value for MB adsorption on PSA, indicating the spontaneous nature of the adsorption reaction (Khan et al. 2015). Similarly, the progression of adsorption is marked by negative entropy change ( $\Delta S$ ) values, implying a reduction in the inherent randomness at the interface between the PSA composite and dye solution (Aouan et al. 2023; Mosoarca et al. 2020; Salvestrini et al. 2022).

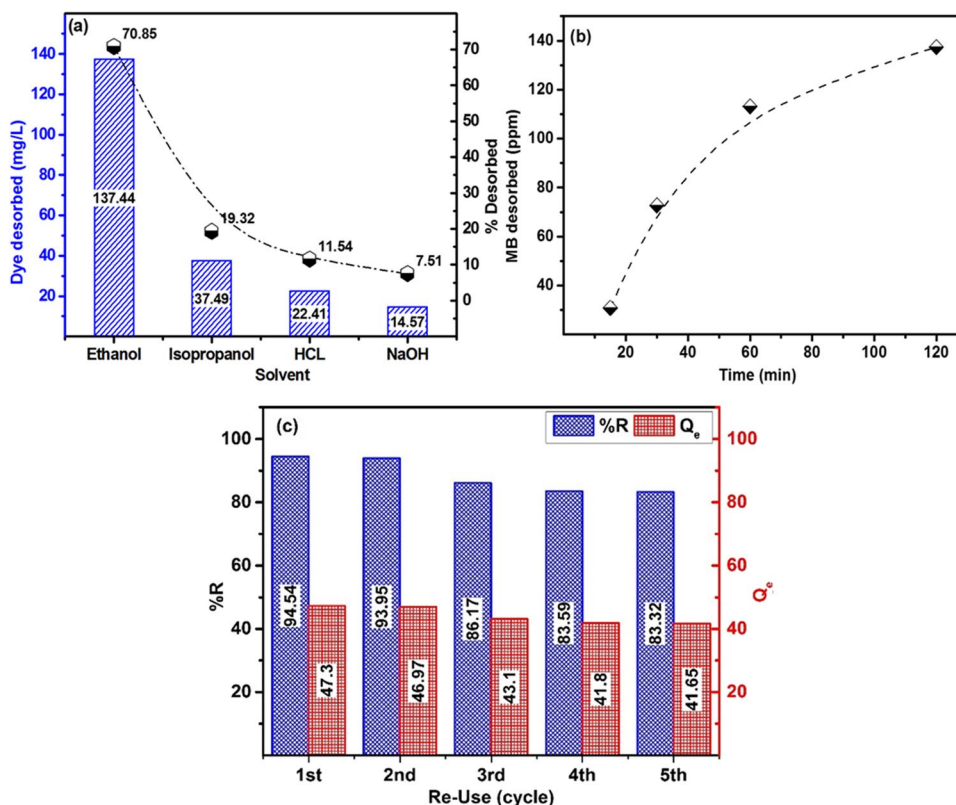
**Desorption and reuse study**

Figure 17 a represents the regeneration of PSA beads and the amount of MB recovered from PSA beads using ethanol, isopropanol, 1 M HCl solution, and 1 M NaOH

solution over a time of 120 min. The % desorption data reveals that 70.85%, 19.32%, 11.54%, and 7.51% of MB were desorbed using ethanol, isopropanol, 1 M HCl solution, and 1 M NaOH solution, respectively. Based on the amount of MB desorbed 137.44 mg/L, 37.49 mg/L, 22.41 mg/L, and 14.57 mg/L of MB was successfully desorbed out PSA beads using ethanol, isopropanol, 1 M HCl, 1 M NaOH solutions, respectively. The desorption of MB, using ethanol as solvent, over a period of 120 min is presented in Fig. 17b representing that 137.44 mg/L of MB was successfully desorbed in 120 min.

The trend in desorption of MB, shown in Fig. 17, agrees with the solubility data of methylene blue in various organic and inorganic solvents. Ethanol is used as a solvent of choice for regeneration of spent adsorbents used for decolourization of MB-contaminated water. Due to the volatile nature of ethanol, ethanol can be easily recovered using low temperature distillation process (Salimi and Roosta 2019). This process will contribute to successful re-use of both ethanol and MB. The PSA beads were successfully reused for five cycles as given in Fig. 17c. There is slight decrease in adsorption of the MB on regenerated PSA compared to freshly prepared one. This decrease in MB adsorption indicates the non availability of some of the adsorption site as all MB did not desorb during desorption process.

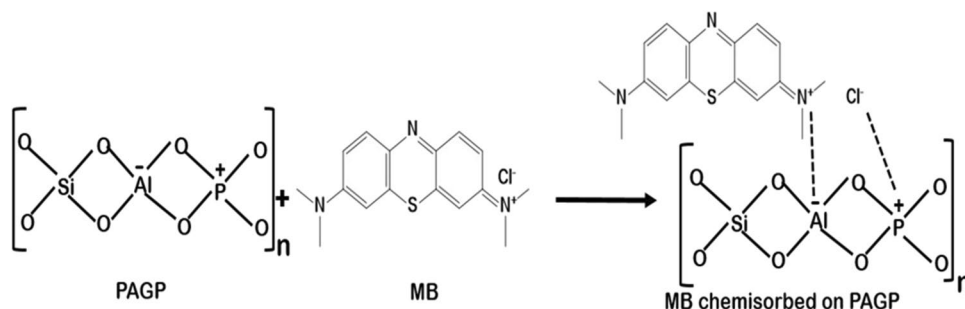
**Fig. 17** Regeneration of PSA adsorbent. **a** Amount of dye desorbed by various solvents. **b** Desorption using ethanol vs time. **c** Re-use of PSA beads for 5 cycles



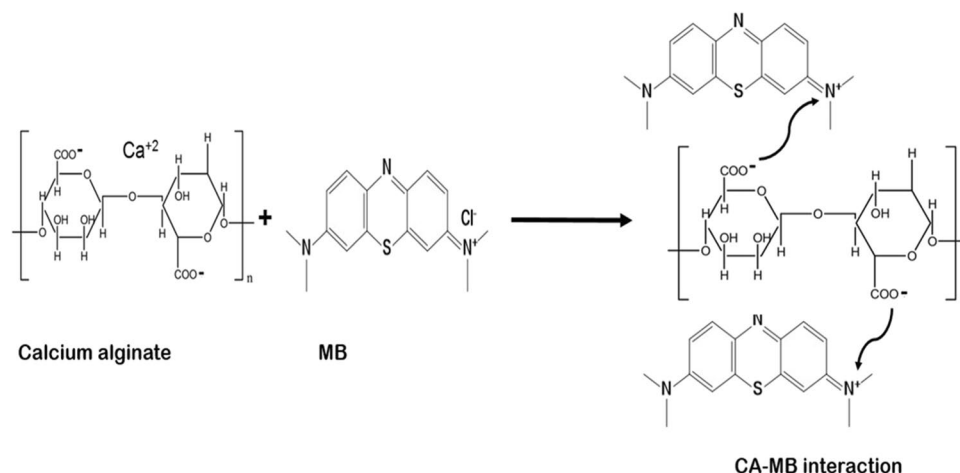
## Adsorption mechanism

The adsorption mechanism can be established using kinetics, isotherm, and thermodynamics parameters obtained by analysis of the adsorption data. As discussed in early sections, the MB adsorption on PSA beads seems to be chemisorption. The finding is supported by good fitting of Langmuir isotherm, PSO kinetics, and negative enthalpy change during adsorption process. There are three types of interactions as given in following reactions. PAGP has negatively charged aluminum and positively charged phosphorus atoms, and these atoms will have strong interactions with MB molecules as shown in reaction Scheme 01 (He et al. 2016; Khan et al. 2015).

**Scheme 1** Attraction of negatively charged aluminum and positively charged phosphorus atoms of PAGP with MB molecules



**Scheme 2** The interaction between the carboxylate anion of alginate with MB<sup>+</sup> cation



**Scheme 3** The interaction between sulfate anion of SLS and MB<sup>+</sup> cation

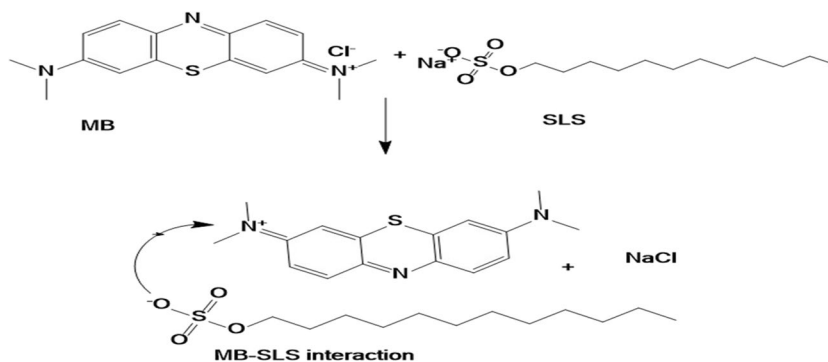




**Table 5** Comparison of this work with previous studies

Raw material	Adsorbent	Activation	Q <sub>max</sub> (mg/g)	Isotherm	Kin. model	Ref
Fly ash	Geopolymer alginate-SLS	H <sub>3</sub> PO <sub>4</sub>	1666.66	Langmuir	PSO	This work
Metakaolin	PAGP	H <sub>3</sub> PO <sub>4</sub>	2.94 and 3.02	Langmuir	PSO	(Khan et al. 2015)
Metakaolin	PAGP	H <sub>3</sub> PO <sub>4</sub>	71.4	Temkin	PSO	(En-Naji et al. 2023)
Metakaolin	Geopolymer	Sodium meta silicate	39.05	Langmuir	PSO	(Candamano et al. 2023)
Pyrophyllite rich clay	Geopolymer	Alkaline	64.10	Langmuir	PSO	(Ettahiri et al. 2023)
Hypergolic coal gangue	Geopolymer	Alkaline	9.4	Langmuir	PSO	(Li et al. 2023)
Coal microsphere	Geopolymer composite	Alkaline	24.6	Langmuir	PSO	(Yan et al. 2018)
ZSM-5 zeolite	Geopolymer foam	Alkaline	8.17–9.82	Langmuir	PSO	(Monjezi and Javanbakht 2023)
Red mud, MK	3D printed geopolymer	Alkaline	19.96	Langmuir	-	(Gonçalves et al. 2023)
MK, alginate	Geopolymer composite	Alkaline	3.2–4.2	-	PSO	(Medri et al. 2020)
Graphene oxide, Alg	Alginate composite	-	181.81	Langmuir	PSO	(Li et al. 2013)
CA, ball milled biochar	Alginate composite	-	1210.7	Langmuir	Ritchie's	(Wang et al. 2019)
Alginate, rice husk	Alginate composite	-	274.9	Freundlich	Fractal Brouers-Sotolongo	(Alver et al. 2020)

## Comparison with previous studies

The adsorptive removal of MB using PSA beads is compared with some of the recent literature reported. Adsorption capacity (mg/g) is considered as the litmus test to estimate the efficiency of an adsorbent. In previous works adsorption capacity in the range of 2.94–71.4 mg/g is achieved by various types of geopolymers, geopolymer foams, and their composites, etc., as given in Table 5. The adsorption capacity achieved by PSA beads is many fold higher than those of the previously reported geopolymer and its composites. The nature of adsorption did not change, as like previous studies Langmuir isotherm and PSO kinetics fitted well on the adsorption data (Khan et al. 2015). The comparison indicates that PSA beads are more effective than various forms of geopolymers, e.g., alkali-activated geopolymers, phosphoric acid-activated geopolymers, geopolymer foam, and 3D-printed geopolymers. As discussed in previous sections, the addition of alginate and SLS resulted in greater enhancement of the adsorption capacity of PSA beads. SLS functionalization of the geopolymer and its composites resulted in enhanced adsorption of MB.

## Conclusions

It is concluded that phosphoric acid geopolymer-SLS-alginate beads have potential to be used as effective adsorbent for methylene blue adsorption. The beads demonstrate effective utilization across a broad pH range, with a preference for neutral pH, given the point of zero charge for the PSA beads

is 7.4. Achieving equilibrium takes approximately 270 min, and a noteworthy trend emerges with temperature variations: there is a remarkable decline in adsorption as temperatures increase. The adsorption capacity increases with increasing dyes concentration as PSA adsorbed 241.14 mg/g of MB at 500 mg/L, 95.81 mg/g at 200 mg/L, and 48.85 mg/g at 100 mg/L concentration. PSA beads have porous structure, amorphous nature, and good thermal stability. The adsorption process follows PSO kinetics ( $R^2=0.999$ ) and Langmuir isotherm ( $Q=1666.66$  mg/g and  $R^2=0.98$ ). A two-step IPD process governs the process of adsorption: first fast step till 30 min followed by slower till 300 min. The adsorption process is thermodynamically exothermic ( $\Delta H = -40.47$  kJ/mol) and energetically favorable ( $\Delta G = -8.198$  to  $-6.014$  kJ mol<sup>-1</sup>). The spent PSA beads can be easily regenerated using ethanol as solvent over a period of 120 min and reused for multiple times. The nature of adsorption is chemisorption where methylene blue reacts with PAGP, calcium alginate, and SLS as confirmed by PSO and IPD models.

Research on the effects of different surfactants, such as cationic, anionic, and neutral surfactants, is recommended. Additional biopolymers, such as chitosan and lignin, should be included in the future study. Finally, additional new contaminants such pesticides, pharmaceuticals, microplastics, and organic compounds may be the focus of this effort in the future.

**Author contribution** All authors contributed to the study conception and design. Material preparation, data collection, analysis, and explanation were performed by Muhammad Irfan Khan. Suriati Sufian, Rashid Shamsuddin, and Muhammad Farooq provided the detailed insight and

guidance related to the research. Nabilah Safi contributed toward manuscript writing and arrangement. The first draft of the manuscript was written by Muhammad Irfan Khan, and all authors contributed in shaping the manuscript. All authors read and approved the final manuscript.

**Funding** Financial support provided by the YUTP grant no. 015PBC-026 in terms of samples analysis, and chemical and equipments' purchase is acknowledged.

## Declarations

**Ethical approval** Not applicable.

**Consent to participate** Not applicable.

**Consent publication** Not applicable.

**Competing interests** The authors declare no competing interests.

## References

- Ahmad ARD, Imam SS, Adnan R, Da Oh W, Latip AFA, Ahmad AAD (2023) Fenton degradation of ofloxacin antibiotic using calcium alginate beads impregnated with Fe<sub>3</sub>O<sub>4</sub>-montmorillonite composite. *Int J Biol Macromol* 229:838–848
- Al-Ghouti MA, Al-Absi RS (2020) Mechanistic understanding of the adsorption and thermodynamic aspects of cationic methylene blue dye onto cellulosic olive stones biomass from wastewater. *Sci Rep* 10:15928
- Almas M, Khan AS, Nasrullah A, Din IU, Fagieh TM, Bakhsh EM, Akhtar K, Khan SB, Khan SZ, Inayat A (2022) Substantial increase in adsorption efficiency of local clay-alginate beads toward methylene blue impregnated with SDS. *Environ Sci Pollut Res* 30(34):81433–81449
- Alver E, Metin AÜ, Brouers F (2020) Methylene blue adsorption on magnetic alginate/rice husk bio-composite. *Int J Biol Macromol* 154:104–113
- Aouan B, Alehyen S, Fadil M, El Alouani M, Saufi H, El Herradi EH, El Makhroukhi F, Taïbi Mh (2023) Development and optimization of geopolymer adsorbent for water treatment: application of mixture design approach. *J Environ Manage* 338:117853
- Benkhaya S, M'rabet S, Lgaz H, El Bachiri A, El Harfi A (2022) Dyes: classification, pollution, and environmental effects, dye biodegradation, mechanisms and techniques. Springer, pp 1–50
- Candamano S, Coppola G, Mazza A, Caranqui JIC, Bhattacharyya S, Chakraborty S, Alexis F, Algieri C (2023) Batch and fixed bed adsorption of methylene blue onto foamed metakaolin-based geopolymer: a preliminary investigation. *Chem Eng Res Des* 197:761–773
- Celerier H, Jouin J, Mathivet V, Tessier-Doyen N, Rossignol S (2018) Composition and properties of phosphoric acid-based geopolymers. *J Non-Cryst Solids* 493:94–98
- Cui X-m, Liu L-p, He Y, Chen J-y, Zhou J (2011) A novel aluminosilicate geopolymer material with low dielectric loss. *Mater Chem Phys* 130:1–4
- Derouiche R, Baklouti S (2021) Phosphoric acid based geopolymerization: effect of the mechanochemical and the thermal activation of the kaolin. *Ceram Int* 47:13446–13456
- Durrani WZ, Nasrullah A, Khan AS, Fagieh TM, Bakhsh EM, Akhtar K, Khan SB, Din IU, Khan MA, Bokhari A (2022) Adsorption efficiency of date palm based activated carbon-alginate membrane for methylene blue. *Chemosphere* 302:134793
- Dutta S, Gupta B, Srivastava SK, Gupta AK (2021) Recent advances on the removal of dyes from wastewater using various adsorbents: a critical review. *Mater Adv* 2:4497–4531
- El-Ashtoukhy ESZ, Amin NK, Abdelwahab O (2008) Removal of lead (II) and copper (II) from aqueous solution using pomegranate peel as a new adsorbent. *Desalination* 223:162–173
- El-Habacha M, Dabagh A, Lagdali S, Miyah Y, Mahmoudy G, Sinan F, Chiban M, Iaich S, Zerbet M (2023) An efficient and adsorption of methylene blue dye on a natural clay surface: modeling and equilibrium studies. *Environ Sci Pollut Res* 1–15
- En-Naji S, Ghazi S, Mabroum H, Mabroum S, Khatib K, Taha Y, Lodeiro IG, Hakkou R (2023) Design of acid-geopolymers based on clays by-products for methylene blue removal from wastewater. *Appl Clay Sci* 245:107126
- Ettahiri Y, Bouna L, Hanna JV, Benlhachemi A, Pilsworth HL, Boudouch A, Bakiz B (2023) Pyrophyllite clay-derived porous geopolymers for removal of methylene blue from aqueous solutions. *Mater Chem Phys* 296:127281
- Gameiro T, Novais RM, Correia CL, Carvalheiras J, Seabra MP, Tarelho LAC, Labrincha JA, Capela I (2021) Role of waste-based geopolymer spheres addition for pH control and efficiency enhancement of anaerobic digestion process. *Bioprocess Biosyst Eng* 44:1167–1183
- Ge Y, Cui X, Liao C, Li Z (2017) Facile fabrication of green geopolymer/alginate hybrid spheres for efficient removal of Cu(II) in water: batch and column studies. *Chem Eng J* 311:126–134
- Gonçalves NP, Olhero SM, Labrincha JA, Novais RM (2023) 3D-printed red mud/metakaolin-based geopolymers as water pollutant sorbents of methylene blue. *J Clean Prod* 383:135315
- Hamdaoui O (2006) Batch study of liquid-phase adsorption of methylene blue using cedar sawdust and crushed brick. *J Hazard Mater* 135:264–273
- He Y, Liu L, He L, Cui X (2016) Characterization of chemosynthetic H<sub>3</sub>PO<sub>4</sub>-Al<sub>2</sub>O<sub>3</sub>-2SiO<sub>2</sub> geopolymers. *Ceram Int* 42:10908–10912
- Katheresan V, Kansedo J, Lau SY (2018) Efficiency of various recent wastewater dye removal methods: a review. *J Environ Chem Eng* 6:4676–4697
- Khan MI, Min TK, Azizli K, Sufian S, Ullah H, Man Z (2015) Effective removal of methylene blue from water using phosphoric acid based geopolymers: synthesis, characterizations and adsorption studies. *RSC Adv* 5:61410–61420
- Khan TA, Chaudhry SA, Ali I (2013) Thermodynamic and kinetic studies of As (V) removal from water by zirconium oxide-coated marine sand. *Environ Sci Pollut Res* 20:5425–5440
- Khapre M, Shekhawat A, Saravanan D, Pandey S, Jugade R (2022) Mesoporous Fe-Al-doped cellulose for the efficient removal of reactive dyes. *Mater Adv* 3:3278–3285
- Kondaveeti S, Petri DF, Jeong HE (2022) Efficiency of air-dried and freeze-dried alginate/xanthan beads in batch, recirculating and column adsorption processes. *Int J Biol Macromol* 204:345–355
- Kumar M, Tamilarasan R (2013) Kinetics and equilibrium studies on the removal of Victoria blue using prosopis juliflora-modified carbon/Zn/alginate polymer composite beads. *J Chem Eng Data* 58:517–527
- Lagergren SK (1898) About the theory of so-called adsorption of soluble substances. *Sven Vetenskapsakad Handlingar* 24:1–39
- Lemougna PN, Wang K-t, Tang Q, Melo UC, Cui X-m (2016) Recent developments on inorganic polymers synthesis and applications. *Ceram Int* 42:15142–15159
- Li X, Liu L, Bai C, Yang K, Zheng T, Lu S, Li H, Qiao Y, Colombo P (2023) Porous alkali-activated material from hypergolic coal gangue by microwave foaming for methylene blue removal. *J Am Ceram Soc* 106:1473–1489

- Li Y, Du Q, Liu T, Sun J, Wang Y, Wu S, Wang Z, Xia Y, Xia L (2013) Methylene blue adsorption on graphene oxide/calcium alginate composites. *Carbohydr Polym* 95:501–507
- Liu G, Hu Z, Guan R, Zhao Y, Zhang H, Zhang B (2016) Efficient removal of methylene blue in aqueous solution by freeze-dried calcium alginate beads. *Korean J Chem Eng* 33:3141–3148
- Lotfy D, El-Sayyad GS, Shehata N (2023) Hexamethylenetetramine functionalized graphene oxide-alginate beads nanocomposite as efficient sorbent for dye from aqueous solution. *Int J Biol Macromol* 228:754–772
- Majd Mozaffari M, Kordzadeh-Kermani V, Ghalandari V, Askari A, Sillanpää M (2022) Adsorption isotherm models. A comprehensive and systematic review (2010–2020). *Sci Total Environ* 812:151334
- Mahmoudian MH, Azari A, Jahantigh A, Sarkhosh M, Yousefi M, Razavinasab SA, Afsharizadeh M, Mohammadi Shahrabi F, Pour Pasandi A, Zeidabadi A, Ilaghinezhad Bardsiri T, Ghasemian M (2023) Statistical modeling and optimization of dexamethasone adsorption from aqueous solution by Fe<sub>3</sub>O<sub>4</sub>@NH<sub>2</sub>-MIL88B nanorods: isotherm, kinetics, and thermodynamic. *Environ Res* 236:116773
- Medri V, Papa E, Lizion J, Landi E (2020) Metakaolin-based geopolymer beads: production methods and characterization. *J Clean Prod* 244:118844
- Mohamed F, Shaban M, Zaki SK, Abd-Elsamie MS, Sayed R, Zayed M, Khalid N, Saad S, Omar S, Ahmed AM, Gerges A, El-Mageed HRA, Soliman NK (2022) Activated carbon derived from sugarcane and modified with natural zeolite for efficient adsorption of methylene blue dye: experimentally and theoretically approaches. *Sci Rep* 12:18031
- Monjezi M, Javanbakht V (2023) A novel foam of geopolymer based on ZSM-5 zeolite fabricated using templating emulsion/chemical foaming method and its application in batch and continuous dye removal systems. *Environ Prog Sustain Energy* 42(4):e14074
- Mosoarca G, Vancea C, Popa S, Gheju M, Boran S (2020) Syringa vulgaris leaves powder a novel low-cost adsorbent for methylene blue removal: isotherms, kinetics, thermodynamic and optimization by Taguchi method. *Sci Rep* 10:17676
- Novais RM, Carvalheiras J, Tobaldi DM, Seabra MP, Pullar RC, Labrincha JA (2019) Synthesis of porous biomass fly ash-based geopolymer spheres for efficient removal of methylene blue from wastewaters. *J Clean Prod* 207:350–362
- Nurddin S, Sufian S, Man Z, Rabat N, Ahmad N (2020) Synthesis of high-porosity hybrid geopolymer/alginate adsorbent for effective removal of methylene blue and optimization of parameters using RSM, IOP Conference Series: Materials Science and Engineering (vol. 991, No. 1, p. 012082). IOP Publishing
- Oladoye PO, Ajiboye TO, Omotola EO, Oyewola OJ (2022) Methylene blue dye: toxicity and potential elimination technology from wastewater. *Results in Engineering* 16:100678
- Otzen C, Liermann H-P, Langenhorst F (2023) Evidence for a rosi-aite-structured high-pressure silica phase and its relation to lamellar amorphization in quartz. *Nat Commun* 14:606
- Papa E, Mor M, Murri AN, Landi E, Medri V (2020) Ice-templated geopolymer beads for dye removal. *J Colloid Interface Sci* 572:364–373
- Pingan H, Mengjun J, Yanyan Z, Ling H (2017) A silica/PVA adhesive hybrid material with high transparency, thermostability and mechanical strength. *RSC Adv* 7:2450–2459
- Pourkhorshidi A, Najimi M, Parhizkar T, Jafarpour F, Hillemeier B (2010) Applicability of the standard specifications of ASTM C618 for evaluation of natural pozzolans. *Cement Concr Compos* 32:794–800
- Prabhakar AK, Mohan BC, Tai MH, Yao Z, Su W, Teo SL-M, Wang C-H (2023) Green, non-toxic and efficient adsorbent from hazardous ash waste for the recovery of valuable metals and heavy metal removal from waste streams. *Chemosphere* 329:138524
- Provis JL (2014) Geopolymers and other alkali activated materials: why, how, and what? *Mater Struct* 47:11–25
- Provis JL, Bernal SA (2014) Geopolymers and related alkali-activated materials. *Annu Rev Mater Res* 44:299–327
- Revellame ED, Fortela DL, Sharp W, Hernandez R, Zappi ME (2020) Adsorption kinetic modeling using pseudo-first order and pseudo-second order rate laws: a review. *Clean Eng Technol* 1:100032
- Salimi A, Roosta A (2019) Experimental solubility and thermodynamic aspects of methylene blue in different solvents. *Thermochim Acta* 675:134–139
- Salvestrini S, Ambrosone L, Kopinke F-D (2022) Some mistakes and misinterpretations in the analysis of thermodynamic adsorption data. *J Mol Liq* 352:118762
- Sharp KG (1998) Inorganic/organic hybrid materials. *Adv Mater* 10:1243–1248
- Shehata N, Sayed ET, Abdelkareem MA (2021) Recent progress in environmentally friendly geopolymers: a review. *Sci Total Environ* 762:143166
- Shen YLaL (2008) From Langmuir kinetics to first- and second-order rate equations for adsorption. *Langmuir* 24:11625–11630
- Siyal AA, Shamsuddin MR, Khan MI, Rabat NE, Zulfiqar M, Man Z, Siame J, Azizli KA (2018) A review on geopolymers as emerging materials for the adsorption of heavy metals and dyes. *J Environ Manage* 224:327–339
- Sun Y, Li Y, Chen B, Wang M, Zhang Y, Chen K, Du Q, Wang Y, Pi X (2022) Methylene blue removed from aqueous solution by encapsulation of bentonite aerogel beads with cobalt alginate. *ACS Omega* 7:41246–41255
- Tanimoto Y, Witono AI, Zheng X, Noro S-i (2023) Simultaneous macroscopic structuring and microscopic structure tuning of a metal-organic framework using alginate bead and different drying conditions. *Microporous Mesoporous Mater* 360:112715
- Thommes M, Kaneko K, Neimark AV, Olivier JP, Rodriguez-Reinoso F, Rouquerol J, Sing KSW (2015) Physisorption of gases, with special reference to the evaluation of surface area and pore size distribution (IUPAC Technical Report). *Pure Appl Chem* 87:1051–1069
- Wang B, Gao B, Wan Y (2019) Comparative study of calcium alginate, ball-milled biochar, and their composites on aqueous methylene blue adsorption. *Environ Sci Pollut Res* 26:11535–11541
- Wang J, Guo X (2022) Rethinking of the intraparticle diffusion adsorption kinetics model: interpretation, solving methods and applications. *Chemosphere* 309:136732
- Wu F-C, Tseng R-L, Juang R-S (2009) Initial behavior of intraparticle diffusion model used in the description of adsorption kinetics. *Chem Eng J* 153:1–8
- Yan S, He P, Jia D, Wang Q, Liu J, Yang J, Huang Y (2018) Synthesis of novel low-cost porous gangue microsphere/geopolymer composites and their adsorption properties for dyes. *Int J Appl Ceram Technol* 15:1602–1614
- Yasir N, Khan AS, Hassan MF, Ibrahim TH, Khamis MI, Nancarrow P (2022) Ionic liquid agar–alginate beads as a sustainable phenol adsorbent. *Polymers* 14:984
- Yousefi M, Nabizadeh R, Alimohammadi M, Mohammadi AA, Mahvi AH (2019) Removal of phosphate from aqueous solutions using granular ferric hydroxide process optimization by response surface methodology. *Desalin Water Treat* 158:290–300

- Yousefi M, Gholami M, Oskoei V, Mohammadi AA, Baziar M, Esrafil A (2021) Comparison of LSSVM and RSM in simulating the removal of ciprofloxacin from aqueous solutions using magnetization of functionalized multi-walled carbon nanotubes: process optimization using GA and RSM techniques. *J Environ Chem Eng* 9:105677
- Yousefi M, Farzadkia M, Mahvi AH, Kermani M, Gholami M, Esrafil A (2024) Photocatalytic degradation of ciprofloxacin using a novel carbohydrate-based nanocomposite from aqueous solutions. *Chemosphere* 349:140972
- Zhuo S-N, Dai T-C, Ren H-Y, Liu B-F (2022) Simultaneous adsorption of phosphate and tetracycline by calcium modified corn stover biochar: performance and mechanism. *Biores Technol* 359:127477
- Zyoud A, Zyoud AH, Zyoud SH, Nassar H, Zyoud SH, Qamhieh N, Hajamohideen A, Hilal HS (2023) Photocatalytic degradation of aqueous methylene blue using ca-alginate supported ZnO nanoparticles: point of zero charge role in adsorption and photodegradation. *Environ Sci Pollut Res* 30(26):68435–68449

**Publisher's Note** Springer Nature remains neutral with regard to jurisdictional claims in published maps and institutional affiliations.

Springer Nature or its licensor (e.g. a society or other partner) holds exclusive rights to this article under a publishing agreement with the author(s) or other rightsholder(s); author self-archiving of the accepted manuscript version of this article is solely governed by the terms of such publishing agreement and applicable law.

## Authors and Affiliations

Muhammad Irfan Khan<sup>1,2</sup> · Suriati Sufian<sup>1,2</sup>  · Rashid Shamsuddin<sup>4</sup> · Muhammad Farooq<sup>3</sup> · Nabilah Saafie<sup>1,2</sup>

✉ Suriati Sufian  
suriati@utp.edu.my

<sup>1</sup> Department of Chemical Engineering, Universiti Teknologi PETRONAS, 32610 Bandar Sri Iskandar, Perak, Malaysia

<sup>2</sup> Centre of Innovative Nanostructures & Nano Devices (COINN), Institute of Autonomous System, Universiti Teknologi PETRONAS, Seri Iskandar, Perak, Malaysia

<sup>3</sup> National Centre of Excellence for Physical Chemistry, University of Peshawar, Peshawar, Pakistan

<sup>4</sup> Department of Chemical Engineering, Faculty of Engineering, Islamic University of Madinah, 42311 Madinah, Saudi Arabia